Compared arsenic removal from aqueous solutions by synthetic mixed oxides and modified natural zeolites

Angélica Heredia[1] · Jenny Gómez Avila[1] · Ariel Vinuesa[1] · Clara Saux[1] · Sandra M. Mendoza[2] · Fernando Garay[3] · Mónica Crivello[1]

Abstract
Layered Double Hydroxides of Mg–Al–Fe and their mixed metallic oxides of high specific surface area were synthesized by the coprecipitation method. A natural zeolite from a regional quarry with high clinoptilolite content was conditioned and modified. Initially, an acid treatment was applied and subsequently Fe(III) was incorporated by the wet impregnation method. Then the prepared solid materials were characterized by XRD, N_2 adsorption–desorption at 77 K, SEM, DRS UV–Vis, and MP-AES to determine their physicochemical properties. Finally, the solid materials were evaluated as adsorbents for arsenic removal in water. The tracking of As and its species concentration at trace levels was carried out by cathodic stripping Square-wave voltammetry, which has proved to be a highly selective and sensitive electrochemical method. High levels of effectiveness in terms of removal were achieved, particularly with the natural zeolites and mixed oxides of highest iron content.

Keywords Arsenic · Mixed oxides · Natural zeolites · Adsorption · Filter

1 Introduction

A serious human health risk is constituted by the presence of arsenic (As) in groundwater. This outcome is associated with closed basins in semiarid and arid climates and aquifers originated from alluvium and geothermal areas (Hernández-Flores et al. 2018). As a consequence of the partial rock dissolution, high concentration of As is frequently found in the area. One of the regions in the world with the highest level of As is placed in Argentina (Kaushik et al. 2018). Considering the 10 μg L^{-1} (Zhu et al. 2018) guideline value provided by the World Health Organization (WHO) for As concentration, an extensive region of our country is out of range.

Arsenic is present in the environment in inorganic and organic forms. The inorganic form is considered to be the most toxic. The two predominant species of inorganic forms of As which are present in natural water are arsenate [As(V)] and arsenite [As(III)]. Moreover, As(III) and As(V) remain dominant in ground and surface waters, respectively (Mahmood et al. 2012). None of them is biodegradable and both can get accumulated through the trophic network (Zhu et al. 2018). Since these species have neither color nor taste, their presence in water is imperceptible. In humans, As is absorbed from the gastrointestinal tract and then transported in blood bounded to sulfhydryl groups of proteins (Mandal et al. 2016). Its regular consumption results toxic for humans, causing a number of diseases such as cancer of skin, blood vessel diseases, high blood pressure and reproductive disorders. These manifestations are called Chronic Endemic Regional Hydroarsenicism (C.E.R.HA.) (Litter et al. 2009).

✉ Angélica Heredia
angelicacheredia@gmail.com

1 CITeQ-CONICET, Facultad Regional Córdoba, Universidad Tecnológica Nacional, Maestro Marcelo López esq. Cruz Roja Argentina, Ciudad Universitaria, X5016ZAA Córdoba, Argentina

2 CONICET, Facultad Regional Reconquista, Universidad Tecnológica Nacional, Reconquista, Argentina

3 INFIQC-CONICET, Departamento de Físico Química, Facultad de Ciencias Químicas, Universidad Nacional de Córdoba, Pabellón Argentina, Ciudad Universitaria, X5000HUA Córdoba, Argentina

Considering the scarcity of water in many of these contaminated places, more efficient, economical and viable treatments should be applied to groundwater in order to satisfy quality and safety parameters. Among the several techniques that are used for arsenic removal from aqueous sources, adsorption keeps growing in number of applications. This is because adsorption has proved to be one of the simplest and most economically feasible processes for water treatment (Peng et al. 2018). Many materials have been tested as adsorbents. Particularly, mixed metallic oxides resulting from the thermal decomposition of Layered Double Hydroxides (LDH) (Evans and Slade 2006) have shown high values of specific surface area (SSA) that favor the interaction between contaminated water and the active sites of the solid's surface. Besides, the mixed metallic oxide could be rehydrated, recovering their laminar structure after aqueous solution exposure (Valente et al. 2000). In this sense, Aredes et al. have reported the effective arsenic removal from contaminated waters using different iron oxide minerals (Aredes et al. 2012). Since the minerals containing Fe-hydroxides have high affinity for both As(III) and As(V) (Pigna et al. 2006; Zhu et al. 2011), Fe-based LDHs are promising candidates for As removal. However, few studies have been carried out on the removal of As by Mg–Fe–LDH (Caporale et al. 2013, 2011; Park and Kim, 2011; Türk et al. 2009) and all of them were devoted to the sorption of As(V) but not of As(III). Furthermore, the effect of foreign ligands on the sorption/desorption of As on/from LDHs has received also some attention, being chloride, carbonate, nitrate, sulphate, selenite, and phosphate the most commonly assessed anions (Caporale et al. 2013; Yang et al. 2005).

Other interesting adsorbent materials, as a function of their properties, are the zeolites. These porous solids offer a high specific surface area and a notorious ionic exchange capacity. Considering that synthetic zeolites could result quite expensive for the As removal process, the natural ones are an interesting option. Their natural abundance, high chemical stability, great specific surface area and low cost, make these solids ideal candidates for environmental sanitation processes (Akbari Sene et al. 2018).

In order to determine As at trace levels in water, electrochemical methods are a feasible alternative. The simple and eventually portable equipment required for those techniques makes them optimal for in situ determinations. Among the different electrochemical methods, cathodic stripping Square-wave voltammetry (CS-SWV) is one of the most adequate techniques considering its high selectivity for As(III), great stability, and sensitivity (Mays and Hussam, 2009).

In this paper, the synthesis and characterization of mixed oxides of Mg–Al–Fe from LDH compounds as well as the modification of natural zeolites with Fe(III) is presented. After their characterization, the capacity of these samples for remediating water sources contaminated with As is evaluated by CS-SWV.

2 Experimental

2.1 Chemicals

All solutions were prepared with ultrapure water (18 MΩ cm) from a Millipore Milli Q system (DI water). Analytical grade reagents: NaOH (Baker, Argentina), HCl (Baker, Argentina), and $Mg(NO_3)_2$, $Al(NO_3)_3$, $Fe(NO_3)_3$, from Sigma-Aldrich, were employed as received.

A 1.00 g L^{-1} arsenic stock solution was prepared by dissolving an appropriate quantity of As_2O_3 (purity $\geq 99.95\%$, Sigma-Aldrich, Argentina). The stock solution was acidified with HCl to pH 2 and stored in a dark bottle to prevent oxidation of As (III). Standard solutions were prepared weekly from the stock solution.

2.2 Synthesis of mixed oxides and modified zeolites

LDHs precursors were obtained by co-precipitation using the low supersaturation method at constant pH = (10.0 ± 0.5). In all cases, a constant molar ratio $[M^{2+}]/[M^{3+}] = 3$ was used, where $[M^{2+}]$ corresponds to the amount of Mg^{2+} and $[M^{3+}]$ to the total amount of Al^{3+} and Fe^{3+}, the composition of each mixture is indicated in Table 1. Co-precipitation was

Table 1 Experimental and theoretical chemical composition of analyzed samples including the respective values of SSA and pore volume (Vp)

Sample	SSA (m² g⁻¹)		Vp (cm³ g⁻¹)	MP-AES % w/w			$\frac{Mg}{Al+Fe}$	Theoretical % w/w		
	PS_x	OS_x		Fe	Al	Mg		Fe	Al	Mg
LDH_4	90	192	0.18[a]	4.0	4.7	21.4	3.6	7.8	11.3	47.4
LDH_8	77	176	0.24[a]	8.3	2.9	20.9	3.4	15.0	7.2	39.1
LDH_{28}	57	95	0.24[a]	28.2	0	30.8	2.5	27.8	0	36.3
ZA_4	104		0.05	6.3	5.8	0.8		4		
ZA_8	56		0.04	10.1	5.1	0.5		8		
ZA_{28}	110		0.06	21.9	3.3	0.3		28		

[a]OS_x samples

performed by mixing the following two solutions: Solution A corresponds to a set of mixtures of $Mg(NO_3)_2$, $Al(NO_3)_3$, and $Fe(NO_3)_3$, each of them dissolved in 150 mL of DI water. The total amount of cations $[M^{2+} + M^{3+}] = 0.7$ M, while the total amount of $[M^{3+}] = 0.17$ M. Solution B corresponds to 150 mL of Na_2CO_3 0.085 M. Both solutions were added simultaneously to 30 mL of DI water at a drip rate of 60 mL h^{-1} while the reaction medium temperature, was maintained at 70 °C. The pH was kept constant by adding small amounts of NaOH 2 M. Each resulting gel was aged for 18 h, then washed with DI water until measuring pH ≈ 7, and finally centrifuged at 2000 rpm. The solid was dried overnight at 90 °C obtaining the precursor materials. Later, the temperature was increased 3 °C min^{-1} up to 450 °C. At this final temperature, each sample was calcined for 9 h in air atmosphere to obtain the respective mixed oxides. The precursor samples were denominated as PS_x, where x is the percentage of iron incorporated in the sample (PS_0, PS_4, PS_8 and PS_{28}). The mixed oxides synthesized from these samples are indicated as (OS_x). Those materials are named As_OS_x, when the OS_x were exposed to arsenic solutions.

Besides, zeolitic materials (Z) were obtained from a natural tuff with high zeolite phase content (clinoptilolite) from Compañía Minera Argentina S.A. (San Juan, Argentina). An acid pretreatment was done to the pristine material in order to remove carbonates and to increase its specific surface area. The procedure consisted in immersing 2.00 g of Z in 500 mL of a 0.04 M sulfuric acid solution at 80 °C for 8 h under vigorous stirring. After that, the solid was filtered and washed with DI water until measuring neutral pH. Finally, the recovered material of acid treated zeolites (ZA) was dried in an oven at 140 °C for 12 h.

Iron (III) was incorporated to this ZA material by wet impregnation. The ZA was then modified with aqueous solutions of different concentrations of $Fe(NO_3)_3$. The protocol consisted in the evaporation of water by using a rotating evaporator at 80 °C connected to a vacuum pump for 10 min. The obtained solid was further dried at 140 °C for 12 h. Finally, the solids were calcined in static oxidant atmosphere at 400 °C (ramp rate: 5 °C/min) for 5 h. Three materials with different Fe(III) were prepared and denoted as ZA_4, ZA_8 and ZA_{28}, according to the expected iron content.

2.3 Characterization

Microwave Plasma-Atomic Emission Spectroscopy (MP-AES) was used for the determination of the metal content in the materials. The measurements were performed with an Agilent 4200 instrument (Agilent, USA). Prior elemental analysis, samples were dissolved by acid digestion in a microwave oven (SCP Science, Canada).

The XRD powder patterns were collected on an X'pert diffractometer (PANanalytical, Netherlands). The conditions used for the zeolitic materials were a scan speed of 5°/min, in a range of 2θ between 7° and 60°, with a step of 0.026°. The scanning of the PS_x and OS_x was performed under a scan speed of 2/3°/min in 2θ. The diffraction patterns were identified by comparison with those included in the software package PCPDFWIN from the International Centre for Diffraction Data (ICDD). The software High Score was utilized for the analysis of the zeolite samples.

UV–Vis diffuse reflectance spectra (DRUV–Vis) were recorded using a Jasco V-650 spectrometer with an integrating sphere in the wavelength range of 200–900 nm. Also a Spectrolon was used as reflectance standard.

N_2 adsorption–desorption isotherms at 77 K were recorded with an ASAP 2020 instrument (Micromeritics, USA), where the specific surface area (SSA) was determined by the Brunauer–Emmett–Teller (BET) method using de N_2 adsorption data. To eliminate the physically adsorbed water, the samples were degassed for 60 min at 200 °C. In the case of OS_x, the treatment was for 60 min at 390 °C. The images of Scanning Electron Microscopy (SEM) were obtained with an accelerating voltage of 20 kV using a JSM-6380 LV (JEOL, Japan) and a Supra 40 (Carl Zeiss, Germany).

2.4 Batch adsorption experiments

The arsenic removal tests were carried out in a batch reactor. For each evaluation, 0.10 g of the selected solid was put in contact with 70 mL of a 170 μg L^{-1} arsenic solution. The experiments were performed at 25 °C under magnetic stirring at different contact times. Once the removal test was finished, the solid fraction exposed to arsenic was filtered through a Whatman paper filter n° 1. The resulting filtrates were evaluated by CS-SWV to assess the remaining amount of As(III).

In the case of mixed oxides, the resulting dried samples (As_OS_x) were analyzed by XRD to evaluate the structure of the used materials.

2.5 Electrochemical detection

Electrochemical measurements were performed with an Autolab (Eco-Chemie, Utrecht, Netherlands), equipped with a PSTAT 30 potentiostat and the GPES 4.3 software package. A static mercury drop (VA 663 Metrohm, Switzerland) with a specific surface area of 0.40 mm^2 was used as the working electrode. A glassy carbon rod was the counter electrode and all the potentials collected are referred to a $Ag_{(s)}|AgCl_{(s)}|KCl_{(aq)}$ (3.00 M) reference electrode.

After extruding a new mercury drop, a pre-concentration step was applied under stirred conditions at the accumulation potential (E_A) for $t_A = 20$ s. The potential was scanned in the negative direction, after a stabilization time of 5 s. The solution was degassed with high-purity argon for 10 min

prior to the measurements and for an additional 20 s before each scan. The argon atmosphere was maintained throughout the experiments. Parameters in CS-SWV experiments were defined as usual and reducing current is considered to be negative (Mayo et al. 2007; Kartinen and Martin, 1995; Goh et al. 2008; Zhang et al. 2016; Feeney and Kounaves 2002; Toor et al. 2015; Jia et al. 2006). Additional data has been included as electronic supplementary material.

3 Results and discussion

3.1 X-ray diffraction

The XRD patterns of the different iron content precursors are shown in Fig. 1a. In all samples, the 2θ peaks 11.62°, 23.38°, 34.43°, 60.5° and 61.8° can be observed. These reflections are related to the diffraction planes (003), (006), (009), (110), and (113), respectively. These planes are characteristic of hydrotalcite-like phase according to the data of the ICDD (PCPDFWIN 70-2151). The reflections assigned to the (003) and (006) planes were used to calculate the basal spacing (d) between the brucite-like sheets. This distance is important because it indicates the size of the charge compensating anions (carbonate or arsenic species). The sample PS_0 presents sharp and well-defined peaks, whereas broader and less intense reflections are observed for the samples with higher iron content. As a result of this, the incorporation of iron in the samples would produce loss of crystallinity in their structures.

In the same figure, the XRD patterns of samples calcined at 450 °C are shown. The reflection planes (003) and (006) disappear due to rupture of the laminar structure in all the samples. As it can be observed, all the patterns show presence of MgO in the periclase phase (PCPDFWIN 78-0430). Also, the presence of hematite Fe_2O_3 (PCPDFWIN 79-1741) indicates that Fe^{3+} ion is crystallized. When the calcination temperature is below 800 °C, the alumina (Al_2O_3) phase
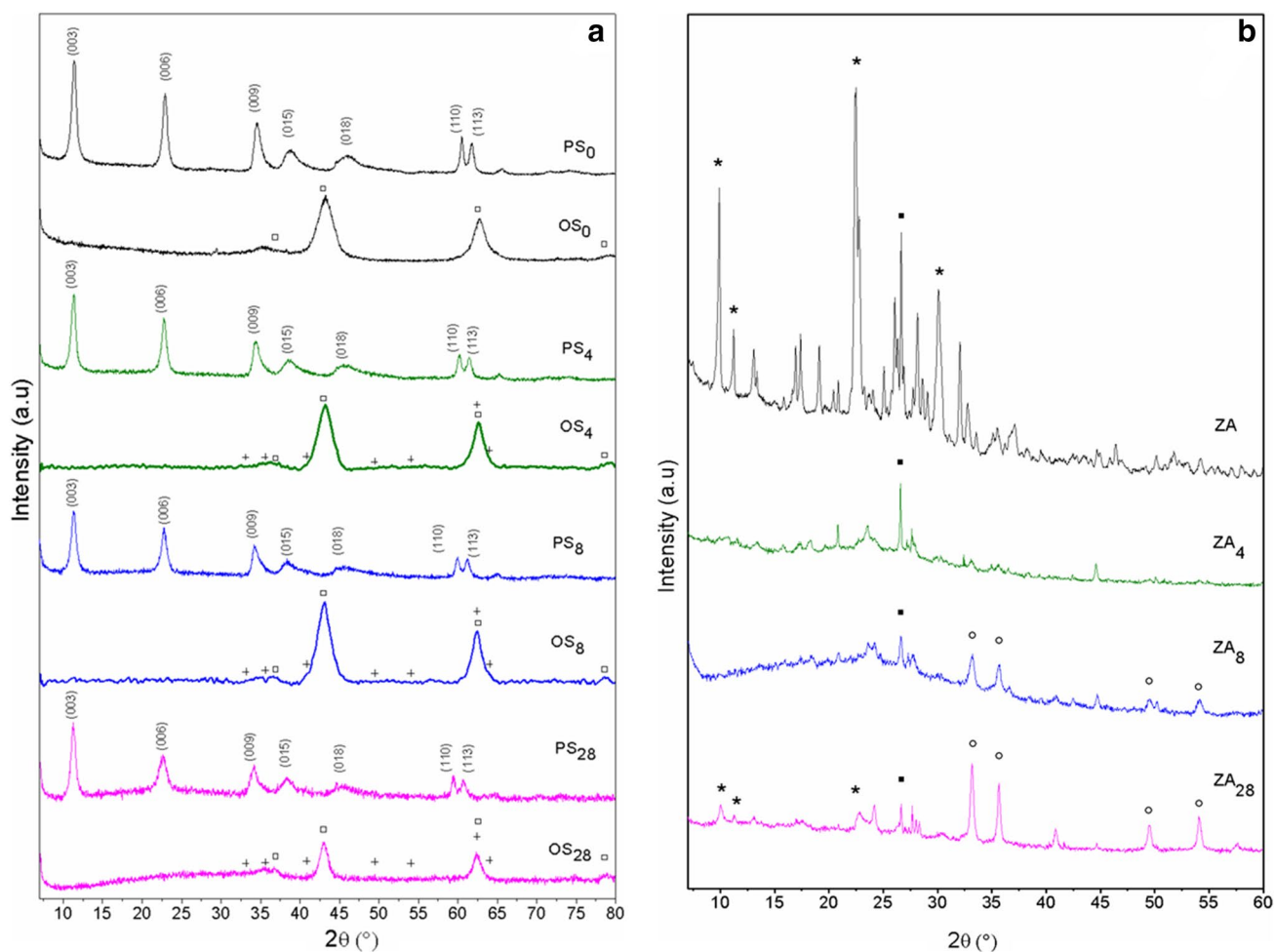
Fig. 1 X-ray diffraction patterns. **a** LDHs precursors and mixed oxides: (opensquare) periclase MgO, and (plus) hematite Fe_2O_3. **b** Natural zeolites: (asterisk) clinoptilolite, (filledsquare) quartz and feldspars, (degree) hematite

adopts an amorphous structure, and diffraction patterns are not observed (Cava et al. 2007).

In Fig. 1b, the patterns of ZA samples modified with different iron content are charted. The characteristic reflections of zeolites, corresponding to the 2θ peaks at 9.87°, 11.21°, 22.37°, and 30.17°, are indicated with (asterisk) and have been chosen to follow the evolution of this phase in the materials. However, those reflections mostly disappeared after the modification of ZA samples with iron. The reflection at 27° (filledsquare) could be assigned to species siliceous such as quartz and feldspars. The samples ZA_8 and ZA_{28} showed reflections at 33.16°, 35.64°, and 54.07°, which are characteristic of hematite like structures. Whereas the evolution of those reflections was proportional to the iron content in samples ZA_8 and ZA_{28}, they were missing in sample ZA_4. In this regard, the iron incorporated to the sample ZA_4 would be present in the form of small iron clusters that were too dispersed to be detected by the XRD analysis (Xie et al. 2015).

3.2 DRUV–Vis-spectroscopy

DRUV–Vis spectra of PS_x, OS_x, and modified zeolites are shown in Fig. 2. The spectra have been deconvoluted into a set of bands that can be assigned to different Fe species. In Fig. 2A all PS_x exhibit a band at ~260 nm. This band could be assigned to the octahedral coordinated Fe^{3+} ions in brucite layered structure (Heredia et al. 2013). The band

observed at ~350 nm has been assigned to small octahedral Fe^{3+} clusters that could be coordinated to other hydroxides (Centi and Vazzana, 1999). Therefore, it is expected that octahedral Fe^{3+} remains outside of the lamellar structure in small oxy-hydroxide structures. The presence of larger iron oxide nanoparticles outside of the lamellar structure was evidenced by the band at 475 nm (Liu et al. 2004; Chmielarz et al. 2006). Therefore, the existence of Fe^{3+}oxides and hydroxides outside the lamellar structure is favored when the iron content in the samples is increased.

Figure 2B shows DRUV–Vis spectra of mixed oxides where the band at 260 nm, previously assigned to octahedral coordinated Fe^{3+}, can also be observed. The band at 340 nm has been assigned to isolated Fe^{3+} in periclase Mg(Fe, Al)O (Heredia et al. 2013). As it was previously indicated, the band at 475 nm corresponds to iron oxide clusters as well as to relatively large iron oxide nanoparticles (Ohishi et al. 2005). In this regard, the increment of iron content would favor not only the presence, but also the size of iron nanoparticles in the sample.

Figure 2C shows DRUV–Vis spectra of zeolites as well as the result of their deconvolution analysis. The spectrum of the sample ZA is characterized by an intense absorption band at 249 nm. However, this band becomes less important when zeolites are modified with iron.

In the case of the iron modified ZA samples (ZA_x), the first maximum of the spectra below 300 nm is attributed to isolated Fe^{3+} ions (Pérez-Ramírez et al. 2004). However, it
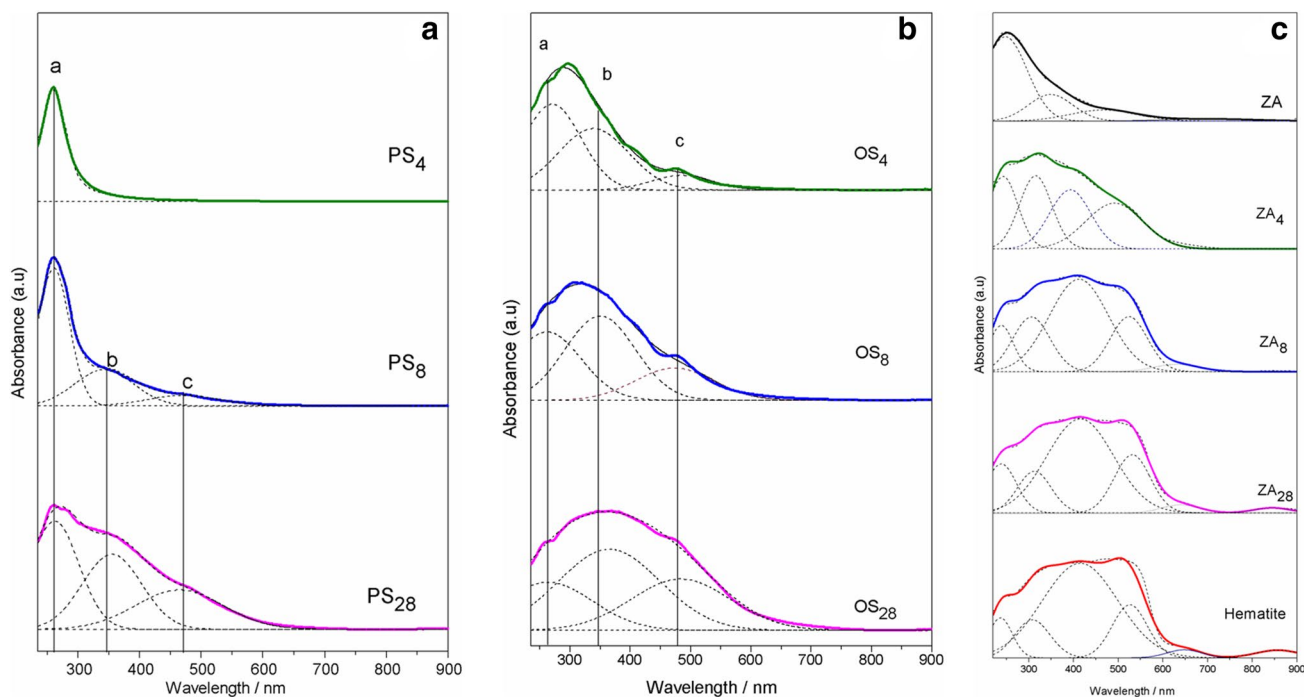
Fig. 2 DRS UV–Vis spectra. **a** LDHs *a* octahedral Fe^{3+}, *b* octahedral Fe^{3+} in small oxy-hydroxides, *c* Fe^{3+} nanoparticles. **b** Mixed oxides: *a* octahedral Fe^{3+}, *b* Fe^{3+} in periclase phase, *c* Fe^{3+} nanoparticles. **c** Natural and modified zeolites

is difficult to determine whether the isolated Fe^{3+} species are in tetrahedral or higher coordination. The broad band between 300 and 500 nm could be assigned to contributions of the d–d transitions of Fe^{3+} in tetrahedral environment (Berlier et al. 2002), and to octahedral Fe^{3+} ions in small oligonuclear clusters (Pérez-Ramírez et al. 2004). The bands observed for wavelengths higher than 500 nm can be attributed to larger α-Fe_2O_3 particles. These bands were only observed for samples with the highest iron content. The presence of these species was also corroborated by XRD patterns and SEM images. It is particularly interesting to notice the similitude between the spectra of ZA_8 and ZA_{28} and that of bulk hematite, which would indicate the prevalence of large α-Fe_2O_3 particles in the modified zeolites.

3.3 Elemental and texture analysis

Table 1 summarizes the chemical compositions determined by MP-AES analysis, as well as the values of SSA and pore volume for the set of precursors, mixed oxides, and modified zeolites.

The experimental Mg, Al, and Fe weight percent values determined for the mixed oxides are lower than theoretical values. Although the experimental molar ratios of Mg/(Al + Fe) decrease with the increment of iron content, those values remain close to the theoretical ones. A behavior quite similar to that described for the OS_x samples is observed from the comparison of the experimental results of MP-AES with the theoretical composition expected for modified zeolitic materials.

N_2 adsorption–desorption isotherms at 77 K for OSx and ZAx samples were performed and some corresponding results are summarized in Table 1. Zeolites show reversible type IV isotherms according to the IUPAC classification with hysteresis loop type H4. This kind of loop is common amongst aggregated crystals of zeolites and some mesoporous zeolites. Iron addition by wet impregnation followed by calcination can reduce the SSA of zeolites due to pore blockage caused by the formation of oxides. This behavior can be observed for samples ZA_4 and ZA_8 where the latter has a considerably lower SSA value. ZA_{28} does not follow this logic and has greater SSA values than ZA_8. SEM images of ZA_{28} show perforated plaque-like structures with greater rugosity and porous structures compared to ZA_4 and ZA_8. This structure could be caused by the higher iron nitrate concentration of the solution, and hence higher acidity, used to make the impregnation. Even when the specific surface area of the pristine material decreases after chemical and thermal treatments, the SSA values found for the ZA_x samples are considerably high to ensure good dispersion of the diverse iron species.

OS_x samples show reversible type II isotherms according to the IUPAC classification. From the analysis of their isotherms we conclude that these materials are slightly porous or macroporous. This is in accordance with results reported by Ramos Guivar et al. (2018) in γ-Fe_2O_3-TiO_2. In addition, it is observed that the values of SSA diminish with the increment of iron concentration of PS_x and OS_x samples. This effect can be assigned to the decrease of amorphous alumina in those samples. In every case, the SSA of each OS_x is greater than that of the precursor. In this regard, the values of SSA for the samples OS_4 and OS_8 increased more than twice due to the calcination of their respective precursors. The increment of SSA for the sample PS_{28} increased only 65%. It is well-known that the gradual isomorphic substitution of Al^{3+} for Fe^{3+} prevents Mg^{2+} incorporation in the brucite layer and consequently distorts the precursor structures (Triantafillidis et al. 2010). Since the ionic radius of Fe^{3+} is bigger than that of Al^{3+}, the structure of those layered double hydroxides is more distorted when Mg^{2+} is displaced by Fe^{3+} ions.

3.4 SEM study

Figure 3 shows micrographs of mixed oxides with different iron content. The samples OS_4 and OS_8 exhibit porous structures with small crystalline domains, while the increment of iron content in the samples induces the formation of bigger and more amorphous structures such as those found in OS_{28}.

The sample OS_{28} shows sintering effects, which are usually associated with samples with low aluminum content (Al_2O_3 amorphous). In this regard, the results are in agreement with the analysis performed by DRUV–Vis spectroscopy and the low SSA observed for the OS_{28}. Moreover, the characteristics of sample OS_{28} would indicate that the interaction of those particles with arsenite ions should take place mostly at the surface of the particles.

The surface of natural zeolite specimens is highly heterogeneous due to the coexistence of the zeolite together with other crystalline and amorphous materials. Crystals of various shapes and sizes, together with amorphous masses, incorporated into friable grains. The HEU-type crystals are normally tabular, platy or coffin-shaped, with sizes that range from 0.1 to 100 µm (Elaiopoulos et al. 2010). Figure 4 shows an image of the zeolite after the acid treatment (ZA) and images corresponding to the samples ZA_4, ZA_8, and ZA_{28}. The sample ZA shows platy structures that were expected for HEU-type crystals. The surface is covered with small and sharp debris of crystals, probably created during the acid treatment. The disordered agglomeration of plates creates large pores through a whole laminar structure. ZA_4 and ZA_8 images resemble each other. Although the platy crystal structure of these samples is similar to the one found in ZA, the XRD analysis indicates that the zeolitic structure for the iron modified samples was severely damaged. Small round shaped formations can be seen on the terraces of the
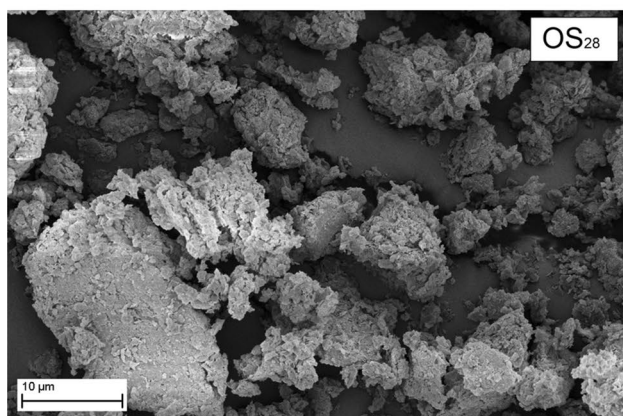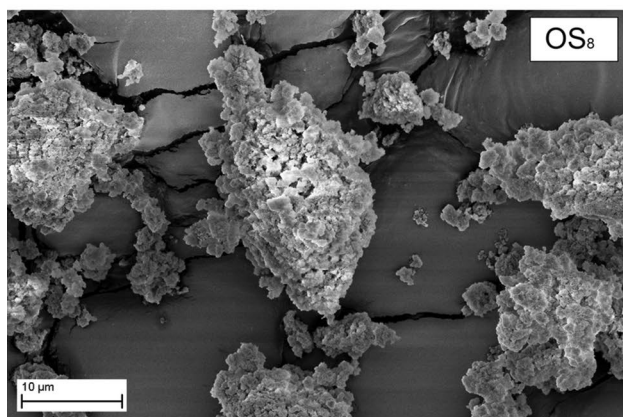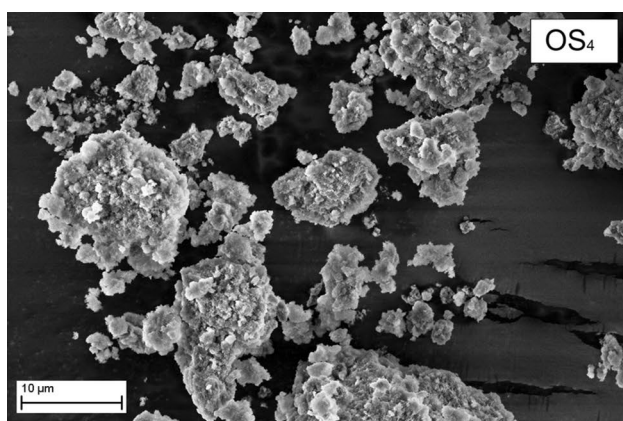
Fig. 3 SEM micrographs of mixed oxides with different iron content

platy structures of the samples ZA_4, ZA_8, and ZA_{28}. Even though these rounded structures are slightly noticeably in the sample ZA_4, they are much more visible in ZA_8 and clearly prevail at the surface of ZA_{28}. We believe, based on the XDR analysis and the UV–Vis DRS results, that these round shaped structures are hematite clusters that have grown in size and number with the increment of iron content in the sample. A clinoptilolite crystal surrounded by perforated plate-like structures can be observed in the micrograph

corresponding to ZA_{28} in Fig. 4. The surface of this sample is much more complex than that of ZA, ZA_4 and ZA_8. It possesses a great number of clusters with different sizes and shapes. In addition, there is a new structure, the perforated plaques, not seen in any of the other samples. These images support the results obtained from the N_2 adsorption–desorption isotherms, in which the sample ZA_{28} has greater specific surface area than ZA_8.

3.5 Arsenic removal by mixed oxides and modified zeolites

3.5.1 Adsorption kinetics

The arsenic removal from aqueous solutions was evaluated for the different OS_x and ZA_x samples. Preliminary analysis performed as a function of time indicated that all samples would have reached their respective adsorption equilibria after being exposed for 10 min to 70 mL of solutions with 170 µg L^{-1} of As(III). Accordingly, the results were recorded after 15 min of contact time to ensure that the adsorption equilibrium has been achieved, see Fig. 5.

The adsorption kinetics was tested against the following models:

(a) A kinetic model of pseudo-first order based on Lagergren's equation (Ho 2004):

$$\frac{dq_t}{d_t} = k_1(q_e - q_t) \tag{1}$$

where k_1 (min^{-1}) is the pseudo-first order adsorption rate constant while q_e (mg g^{-1}) and q_t (mg g^{-1}) indicate the amount of adsorbate per g of adsorbent at equilibrium and at any time t, respectively. The integrated form of Eq. (1) is:

$$\ln(q_e - q_t) = \ln(q_e) - k_1 t \tag{2}$$

Where k_1 is the slope and $\ln(q_e)$ the intercept in a plot of $\ln(q_e - q_t)$ versus t.

(b) A kinetic model of pseudo-second order where it is assumed that the number of active sites on the adsorbent directly influences the reaction rate, Eq. (3) (Ho and McKay 1999). The mathematical expression of this kinetic model is:

$$\frac{dq_t}{d_t} = k_2(q_e - q_t)^2 \tag{3}$$

where k_2 (g mg^{-1} min^{-1}) is the pseudo-second order adsorption rate constant. The integrated form of Eq. (3) can be expressed as:
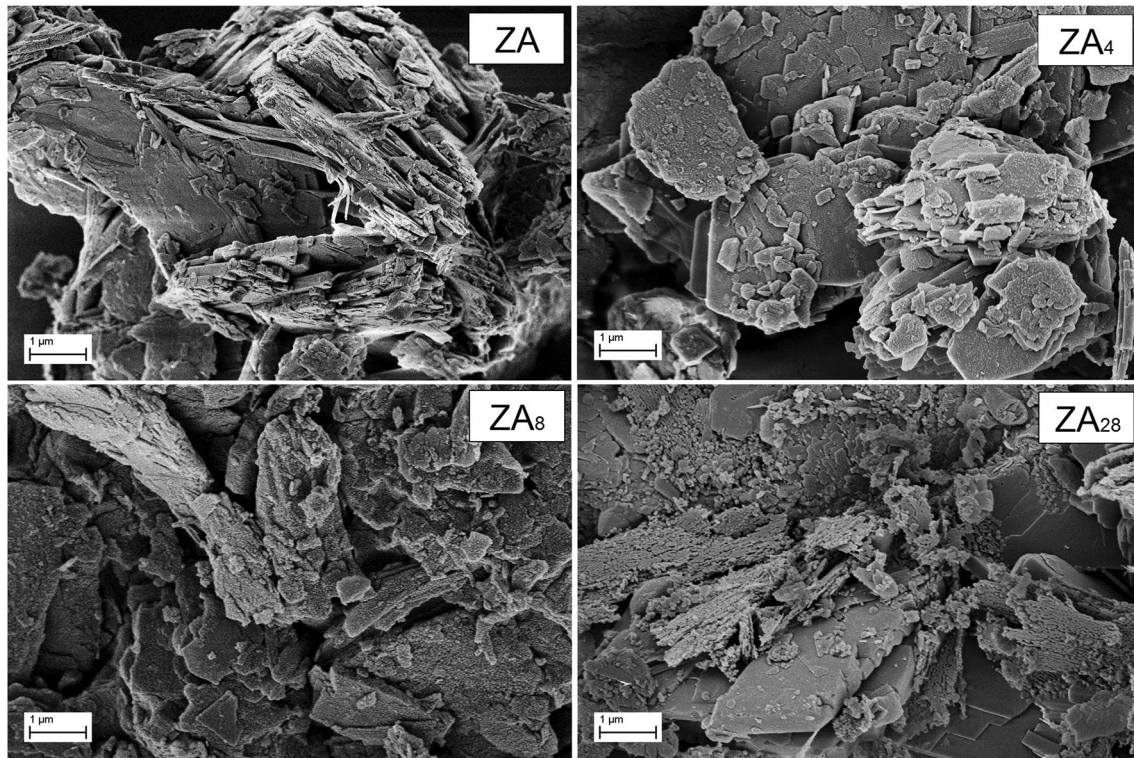
Fig. 4 SEM micrographs of the treated zeolitic matrix with different iron content
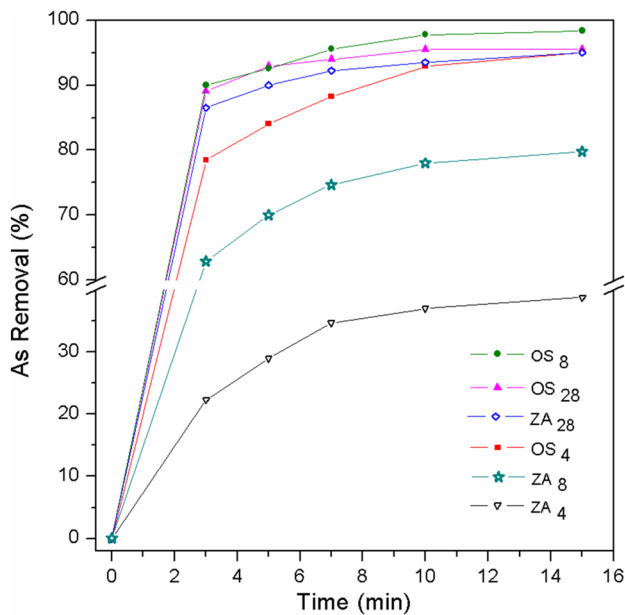

Fig. 5 As (III) removal (%) versus Time (min) for OS_x and ZA_x samples

$$\frac{t}{q_t} = \frac{1}{k_2 q_e^2} + \frac{t}{q_e} \tag{4}$$

Table 2 lists the parameters obtained from fitting experimental data with the models represented by Eqs. (2) and (4). As it can be observed, the analyses performed with the pseudo-second order model show very good correlation values for all samples. The values of k_2 increase with the content of Fe of mixed oxides and modified zeolitic materials, indicating that the adsorption kinetics of As(III) increases with the number of active sites placed at the surface of the samples. In this regard, for OS_x samples the surface-active sites would be hematite nanostructures, while the inner active sites would involve Fe(III) associated to restructured LDH. According to the q_e values obtained from the model of pseudo-second order adsorption kinetics, all samples would have practically achieved their respective adsorption equilibria. Therefore, experimental q_e values are very similar to theoretically expected values of this apparent adsorption constant. All mixed oxides present practically the same q_e, because they have extracted most of soluble As(III). Additional data associated with the adsorption kinetics has been included as electronic supplementary material.

With regards to the modified zeolitic materials, the samples ZA_4 and ZA_8 showed lower adsorption capacity than the mixed oxides. This fact would point out that these samples have still regions of their surface that has not been covered with hematite deposits. The sample ZA_{28}, however, presents practically the same values of q_e than mixed oxides,

Table 2 Kinetic analysis of data with pseudo-first and pseudo-second order models

Sample	Pseudo first order			Pseudo second order			Experimental
	k_1 (min^{-1})	R^2	q_e (mg g^{-1})	K_2 (g mg^{-1} min^{-1})	R^2	q_e (mg g^{-1})	q_e (mg g^{-1})
OS$_4$	2.91	0.878	0.920	8.72	0.999	0.121	0.114
OS$_8$	2.08	0.943	0.927	20.38	0.999	0.121	0.118
OS$_{28}$	1.34	0.928	0.758	34.89	0.999	0.117	0.115
ZA$_4$	3.21	0.996	1.114	6.55	0.992	0.055	0.046
ZA$_8$	3.34	0.943	0.963	7.40	0.999	0.105	0.097
ZA$_{28}$	2.52	0.858	1.032	21.70	0.999	0.116	0.114

indicating that the zeolitic material has been sheltered by hematite nanostructures and that it provides a suitable scaffold for them.

3.5.2 Influence of pH on As(III) removal

The pH value was monitored during the experiments of arsenic adsorption. The addition of OS$_x$ samples shifted the former pH of arsenite solutions from 3.8 to approximately 9. However, the addition of ZA$_x$ changed the pH of the arsenite solution from 3.8 to about 4.1. Irrespectively of the pH achieved, all samples showed significant capacity for As removal.

The effect of pH on arsenic removal was analyzed for samples OS$_{28}$ and ZA$_{28}$. The removal conditions were the same as those carried out in batch removal. Each suspension was shaken for 5 min at room temperature, but keeping a constant pH by dropwise addition of 0.01 M HCl or 0.01 M NaOH. Even when the surface charge of the adsorbent was affected by the pH variations, As removal capacity was not significantly affected. In the case of OS$_{28}$, just a 10% of reduction on arsenite removal capacity was obtained when pH goes from 8 to 10. While at lower pH values the percentage of removal remained almost constant around 95%. A similar trend was found for ZA$_{28}$.

Although the greatest As(III) removal was obtained at acid pH values, the experiments were carried out at natural pH conditions considering the eventual use of these materials in a house filter setting.

3.5.3 Influence of Fe content in the samples

The OS$_x$ samples have the capacity for recovering the structure of their respective precursors (PS$_x$) when they are exposed to aqueous solutions or humid atmospheres. This property is referred to as memory effect. The analysis of XRD patterns of the different OS$_x$ collected after being used for removal reactions is shown in Fig. 6. Those XRD patterns indicate that the samples As_OS$_4$ and As_OS$_8$ reconstitute their precursor structures, while the sample As_OS$_{28}$ keeps its spinel and hematite structures. Thus, the obtained
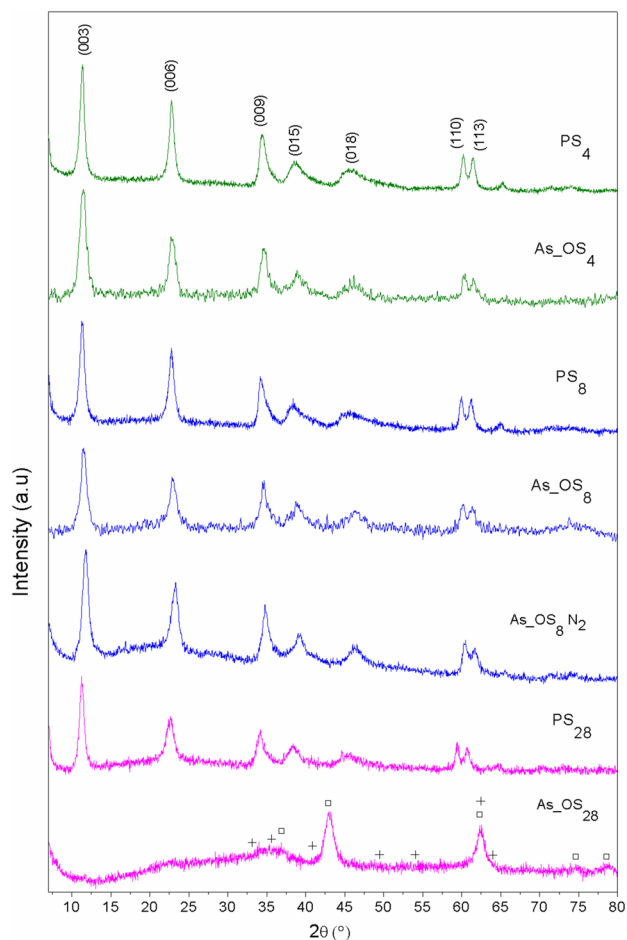
Fig. 6 X-ray diffraction patterns of mixed oxides after arsenic adsorption. Diffraction planes of hydrotalcite-like phases are indicated. (opensquare) periclase MgO, and (plus) hematite Fe$_2$O$_3$

results would point out that neither water nor arsenite ions can reconstitute the layered double hydroxide structure in the OS$_{28}$ sample. It is well-know that the absence of amorphous Al$_2$O$_3$ prevents the LDH reconstruction (Vaccari 1998).

It is well-known that dissolved CO$_2$ could be responsible of LDH structure recovery. As a result, the incorporation of As in the interlayer space of LDH was studied under N$_2$

atmosphere, to prevent the presence of competing anionic species, such as those coming from dissolved CO_2. According to the XRD pattern shown in Fig. 6, the sample OS_8 recovers its LDH structure in the absence of carbonate species ($As\_OS_8\_N_2$). This result would indicate that the arsenite ions can be housed between the sheets of reconstituted LDH structure.

In order to assess and quantify the contribution of the iron species to the adsorption process, removal tests were carried out maintaining the same test conditions previously mentioned with mixed oxides of Mg and Al, but without iron. This sample (OS_0) removed only 77% of arsenite ion from 70 mL of a solution with 170 $\mu g\,L^{-1}$ As(III); while samples OS_4, OS_8 and OS_{28} removed more than 95% of the initial arsenite concentration, despite the different iron content. This may be assigned to a low initial arsenic concentration that prevents the saturation all active sites.

Although this result is well-known, this experiment was carried out for comparing the effect of iron oxides added to zeolitic adsorbents. In this regard, from the data in Fig. 5 it can be clearly deduced that iron oxides also play an important role when they are present in zeolitic adsorbents. The arsenic uptake capacity of these samples increases with their iron content, being ZA_{28} the most efficient. The experiments conducted with ZA removed only 25% of arsenite ion from 70 mL of 170 $\mu g\,L^{-1}$ As(III). Considering that the zeolitic framework has a negative charge introduced by tetrahedrally coordinated aluminium, low adsorption values were expected for this unmodified material.

From the analysis of the above results, the presence of iron oxide in the hematite phase would be responsible of the arsenic adsorption capacity of ZA_x materials. Although the data of Table 2 indicate that the mechanism of adsorption behaves according a pseudo-second order kinetic model, the complexity of the interactions between the termination groups of hematite and the adsorbates can be overwhelming. Eggleston et al. (2003) point out about the growing complexity of the models used in adsorption mechanisms. In their study about the structure of hematite surfaces in aqueous media, they concluded that there is a coexistence of Fe- and O-terminations on (001) hematite surfaces. Moreover, these terminations are dynamic and the adsorbates could influence them. Thus, previous treatments as well as the history of each material would play a key role in the adsorption mechanism.

Mamindy-Pajany et al. (2011) studied the adsorption of As(V) on several iron species, including hematite. They used a sample of commercial hematite with a SSA of 1.66 $m^2\,g^{-1}$ and calculated that the pH for the point of zero charge (pH_{PZC}) was close to 8.1. This fact favors the adsorption of hydroxy species of As that interact mostly by hydrogen-bond reactions with the surface. This could be also the case of samples ZA_x, where the solution pH remained practically unchanged. Taking into account that bulk hematite has low SSA, ZA can be considered as an effective scaffold for dispersing hematite nanoclusters and thus for enhancing their arsenic adsorption capacity.

In this work, it was observed very good adsorption of As(III) species in presence of nanoclusters of hematite disposed onto ZA samples, see Fig. 5. The As(III) adsorption capacity of ZA_x increased with the amount of iron content. An increasing As removal from OS_0 to the set of OS_4, OS_8 and OS_{28} samples was observed, without a great removing variation between the samples with iron incorporation.

4 Conclusions

A set of mixed metallic oxides, layered double hydroxides, and modified natural zeolites were prepared, characterized and then compared by using several physicochemical techniques. All materials can be used in a filtering system for As removal. The As removal capacity was studied in a batch reactor at different contact times. The maximum arsenic removal values were achieved with the samples OS_8 and ZA_{28}.

With regards to the structure of OS_x, the presence of amorphous Al_2O_3 promotes the dispersion of iron species and increases the specific surface area. DRUV–Vis analysis showed that Fe^{+3} ions can be found in octahedral coordination environments, while SEM micrographs evidenced the formation of clusters and aggregates of particles according to the increment of the iron content in the solid.

In the case of ZA_x materials, considerable loss of crystallinity after the acid and thermal treatment was observed. SEM images, however, indicated that iron oxide was adequately dispersed on the surface of those samples. According to DRUV–Vis spectra, Fe^{3+} was found in tetrahedral and octahedral environments that are consistent with hematite nanostructures identified by XRD.

The As removal capacity of synthetic and natural materials was evaluated by CS-SWV. The electrochemical technique was optimized for the quantification of As(III) and the signal resulting from all filtrated materials consisted of a single peak corresponding to the reduction of analyte. The incorporation of iron in synthetic and natural materials showed very promising results. On the one hand, experimental data indicated that OS_x materials restore their structures of layered double hydroxides when they are exposed to water and have the ability for retaining arsenite ions into the resulting interlayer spaces. On the other hand, the surface of ZA_x materials can be covered with hematite nanoclusters that significantly increase their capacity for adsorbing As(III). In consequence, it would be interesting to deposit OS_x on the surface of ZA samples to study if there is any synergy between these two adsorption mechanisms.

Another possibility would be the development of a two-step continuous filtering system where the extraordinary capacity for As removal of OS_x and the low cost of ZA_x materials is combined. First, water polluted with high arsenic concentration should be treated with the inexpensive iron modified natural zeolites. Second, the remaining As species could be practically eliminated by using OS_x materials. The use of ZA_x will notably extend the useful life of OS_x. Ideally, the resulting filtered groundwater should fulfill the WHO guidelines.

References

Akbari Sene, R., Sharifnia, S., Moradi, G.R.: On the impact evaluation of various chemical treatments of support on the photocatalytic properties and hydrogen evolution of sonochemically synthesized TiO_2/Clinoptilolite. Int. J. Hydrog. Energy **43**, 695–707 (2018)

Aredes, S., Klein, B., Pawlik, M.: The removal of arsenic from water using natural iron oxide minerals. J. Clean. Prod. **29–30**, 208–213 (2012)

Berlier, G., Spoto, G., Fisicaro, P., Bordiga, S., Zecchina, A., Giamello, E., Lamberti, C.: Co-ordination and oxidation changes undergone by iron species in Fe–silicalite upon template removal, activation and interaction with N_2O: an in situ X-ray absorption study. Microchem. J. **71**, 101–116 (2002)

Caporale, A.G., Pigna, M., Dynes, J.J., Cozzolino, V., Zhu, J., Violante, A.: Effect of inorganic and organic ligands on the sorption/desorption of arsenate on/from Al–Mg and Fe–Mg layered double hydroxides. J. Hazard. Mater. **198**, 291–298 (2011)

Caporale, A.G., Pigna, M., Azam, S.M.G.G., Sommella, A., Rao, M.A., Violante, A.: Effect of competing ligands on the sorption/desorption of arsenite on/from Mg–Fe layered double hydroxides (Mg–Fe–LDH). Chem. Eng. J. **225**, 704–709 (2013)

Cava, S., Tebcherani, S.M., Souza, I.A., Pianaro, S.A., Paskocimas, C.A., Longo, E., Varela, J.A.: Structural characterization of phase transition of Al_2O_3 nanopowders obtained by polymeric precursor method. Mater. Chem. Phys. **103**, 394–399 (2007)

Centi, G., Vazzana, F.: Selective catalytic reduction of N_2O in industrial emissions containing O_2, H_2O and SO_2: behavior of Fe/ZSM-5 catalysts. Catal. Today **53**, 683–693 (1999)

Chmielarz, L., Kustrowski, P., Dziembaj, R., Cool, P., Vansant, E.: Catalytic performance of various mesoporoussilicas modified with copper or iron oxides introduced by different ways in the selective reduction of NO by ammonia. Appl. Catal. A **62**, 369–380 (2006)

Eggleston, C.M., Stack, A.G., Rosso, K.M., Higgins, S.R., Bice, A.M., Boese, S.W., Pribyl, R.D., Nichols, J.J.: The structure of hematite (-Fe_2O_3) (001) surfaces in aqueous media: scanning tunneling microscopy and resonant tunneling calculations of coexisting O and Fe terminations. Geochim. Cosmochim. Acta **67**, 985–1000 (2003)

Elaiopoulos, K., Perraki, Th, Grigoropoulou, E.: Monitoring the effect of hydrothermal treatments on the structure of a natural zeolite through a combined XRD, FTIR, XRF, SEM and N_2-porosimetry analysis. Micropor. Mesopor. Mat. **134**, 29–43 (2010)

Evans, D.G., Slade, R.C.T.: Structural aspects of layered double hydroxides. In: Duan, X., Evans, D.G. (eds.) Layered Double Hydroxides. Springer, Berlin (2006)

Feeney, R., Kounaves, S.P.: Voltammetric measurement of arsenic in natural waters. Talanta **58**, 23–31 (2002)

Goh, K.H., Lim, T.T., Dong, Z.: Application of layered double hydroxides for removal of oxyanions: a review. Water Res. **42**, 1343–1368 (2008)

Heredia, A.C., Oliva, M.I., Agú, U., Zandalazini, C.I., Marchetti, S.G., Herrero, E.R., Crivello, M.E.: Synthesis, characterization and magnetic behavior of Mg–Fe–Al mixed oxides based on layered double hydroxide. J. Magn. Magn. Mater. **342**, 38–46 (2013)

Hernández-Flores, H., Pariona, N., Herrera-Trejo, M., Hdz-García, H.M., Mtz-Enriquez, A.I.: Concrete/maghemite nanocomposites as novel adsorbents for arsenic removal. J. Mol. Struct. **1171**, 9–16 (2018)

Ho, Y.S., McKay, G.: Pseudo-second order model for sorption processes. Process Biochem. **34**, 451–465 (1999)

Ho, Y.S.: Citation review of Lagergren kinetic rate equation on adsorption reactions. Scientometrics **59**, 171–177 (2004)

Jia, Z., Simm, A.O., Dai, X., Compton, R.G.: The electrochemical reaction mechanism of arsenic deposition on an Au(111) electrode. J. Electroanal. Chem. **587**, 247–253 (2006)

Kartinen, E.O., Martin, C.J.: An overview of arsenic removal processes. Desalination **103**, 79–88 (1995)

Kaushik, V., Duan, Y., Jung, B., Batchelor, B., Abdel-Wahab, A.: Arsenic removal using advanced reduction process with dithionite/UV—a kinetic study. J. Water Proc. Eng. **23**, 314–319 (2018)

Litter, M.I., Armienta, M.A., Farías, S.: Metodologías analíticas para la determinación y especiación de arsénico en aguas y suelos. CYTED, Buenos Aires (2009)

Liu, S., Wang, Q., Van Der Voort, P., Cool, P., Vansant, E., Jiang, M.: Magnetism of iron-containing MCM-41 spheres. J. Magn. Mater. **280**, 31–36 (2004)

Mamindy-Pajany, Y., Hurel, C., Marmier, N., Roméo, M.: Arsenic (V) adsorption from aqueous solution onto goethite, hematite, magnetite and zero-valent iron: effects of pH, concentration and reversibility. Desalination **281**, 93–99 (2011)

Mandal, P., Debbarma, S.R., Saha, A., Ruj, B.: Disposal problem of arsenic sludge generated during arsenic removal from drinking water. Procedia Environ. Sci. **35**, 943–949 (2016)

Mayo, J.T., Yavuz, C., Yean, S., Cong, L., Shipley, H., Yu, W., Falkner, J., Kan, A., Tomson, M., Colvin, V.L.: The effect of nanocrystalline magnetite size on arsenic removal. Sci. Techol. Adv. Mater. **8**, 71–75 (2007)

Mahmood, T., Din, S.U., Naeem, A., Mustafa, S., Waseem, M., Hamayun, M.: Adsorption of arsenate from aqueous solution on binary mixed oxide of iron and silicon. Chem. Eng. J. **192**, 90–98 (2012)

Mays, D., Hussam, A.: Voltammetric methods for determination and speciation of inorganic arsenic in the environment—a review. Anal. Chim. Acta **646**, 6–16 (2009)

Ohishi, Y., Kawabata, T., Shishido, T., Takaki, K., Zhang, Q., Wang, Y., Nomura, K., Takehira, K.: Mg–Fe–Al mixed oxides with mesoporous properties prepared from hydrotalcite as precursors: catalytic behavior in ethylbenzene dehydrogenation. Appl. Catal. A **288**, 220–231 (2005)

Park, J.Y., Kim, J.H.: Characterization of adsorbed arsenate on amorphous and nano crystalline MgFe-layered double hydroxides. J. Nanopart. Res. **13**, 887–894 (2011)

Peng, X., Zhao, Y., Yang, T., Yang, Y., Liu, H.: One-step and acid free synthesis of γ-Fe_2O_3/SBA-15 for enhanced arsenic removal. Microp. Mesop. Mater. **258**, 26–32 (2018)

Pérez-Ramírez, J., Kumar, M.S., Brückner, A.: Reduction of N_2O with CO over FeMFI zeolites: influence of the preparation method on the iron species and catalytic behavior. J. Catal. **223**, 13–27 (2004)

Pigna, M., Krishnamurti, G.S.R., Violante, A.: Kinetics of arsenate sorption-desorption from metal oxides: effect of residence time. Soil Sci. Soc. Am. J. **70**, 2017–2027 (2006)

Ramos Guivar, J., Bustamante, A., Gonzalez, J.C., Sanches, E., Morales, M.A., Raez, M.A., López-Muñoz, M.J., Arencibia, A.: Adsorption of arsenite and arsenate on binary and ternary magnetic nanocomposites with high iron oxide content. Appl. Surf. Sci. **454**, 87–100 (2018)

Toor, S.K., Devi, P., Bansod, B.K.S.: Electrochemical detection of trace amount of arsenic (III) at glassy carbon electrode modified with Au/Fe_3O_4 nanocomposites. Aquatic. Procedia **4**, 1107–1113 (2015)

Triantafillidis, K., Peleka, E., Komvokis, V., Mavros, P.: Iron-modified hydrotalcite-like materials as highly efficient phosphate sorbents. J. Colloid Interface Sci. **342**, 427–443 (2010)

Türk, T., Alp, I., Deveci, H.: Adsorption of arsenate from water using Mg–Fe based hydrotalcite (FeHT). J. Hazard. Mater. **171**, 665–670 (2009)

Vaccari, A.: Preparation and catalytic properties of cationic and anionic clays. Catalysis Today **41**(1–3), 53–71 (1998)

Valente, J., Figueras, F., Gravelle, M., Kumbhar, P., Lopez, J., Besse, J.: Basic properties of the mixed oxides obtained by thermal decomposition of hydrotalcites containing different metallic compositions. J. Catal. **189**, 370–381 (2000)

Xie, P., Luo, Y., Ma, Z., Huang, C., Gao, Z.: Catalytic decomposition of N_2O over Fe-ZSM-11 catalysts prepared by different methods: nature of active Fe species. J. Catal. **330**, 311–322 (2015)

Yang, L., Shahrivari, Z., Liu, P.K.T., Sahimi, M., Tsotsis, T.T.: Removal of trace levels of arsenic and selenium from aqueous solutions by calcined and uncalcined layered double hydroxides (LDHs). Ind. Eng. Chem. Res. **44**, 6804–6815 (2005)

Zhang, B., Liu, J., Ma, X., Zuo, P., Ye, B.C., Li, Y.: Ultrasensitive and selective assay of glutathione species in arsenic trioxide-treated leukemia HL-60 cell line by molecularly imprinted polymer decorated electrochemical sensors. Biosens. Bioelectron. **80**, 491–496 (2016)

Zhu, J., Pigna, M., Cozzolino, V., Caporale, A.G., Violante, A.: Sorption of arsenite and arsenate on ferrihydrite: effect of organic and inorganic ligands. J. Hazard. Mater. **189**, 564–571 (2011)

Zhu, N., Qiao, J., Ye, Y., Yan, T.: Synthesis of mesoporous bismuth-impregnated aluminum oxide for arsenic removal: adsorption mechanism study and application to a lab-scale column. J. Environ. Manag. **211**, 73–82 (2018)